JACS
JOURNAL OF THE AMERICAN CHEMICAL SOCIETY
Article
pubs.acs.org/JACS

Turning On and Off Photoinduced Electron Transfer in Fluorescent Proteins by π-Stacking, Halide Binding, and Tyr145 Mutations

Alexey M. Bogdanov,[†,‡,#] Atanu Acharya,[§,#] Anastasia V. Titelmayer,[†] Anastasia V. Mamontova,[†] Ksenia B. Bravaya,[∥] Anatoly B. Kolomeisky,[⊥] Konstantin A. Lukyanov,[*,†,‡] and Anna I. Krylov[*,§]

[†]Shemiakin-Ovchinnikov Institute of Bioorganic Chemistry, Moscow 117997, Russia
[‡]Nizhny Novgorod State Medical Academy, Nizhny Novgorod 603005, Russia
[§]Department of Chemistry, University of Southern California, Los Angeles, California 90089-0482, United States
[∥]Department of Chemistry, Boston University, Boston, Massachusetts 02215, United States
[⊥]Department of Chemistry, Rice University, Houston, Texas 77251-1892, United States

Supporting Information

ABSTRACT: Photoinduced electron transfer in fluorescent proteins from the GFP family can be regarded either as an asset facilitating new applications or as a nuisance leading to the loss of optical output. Photooxidation commonly results in green-to-red photoconversion called oxidative redding. We discovered that yellow FPs do not undergo redding; however, the redding is restored upon halide binding. Calculations of the energetics of one-electron oxidation and possible electron transfer (ET) pathways suggested that excited-state ET proceeds through a hopping mechanism via Tyr145. In YFPs, the π-stacking of the chromophore with Tyr203 reduces its electron-donating ability, which can be restored by halide binding. Point mutations confirmed that Tyr145 is a key residue controlling ET. Substitution of Tyr145 by less-efficient electron acceptors resulted in highly photostable mutants. This strategy (i.e., calculation and disruption of ET pathways by mutations) may represent a new approach toward enhancing photostability of FPs.

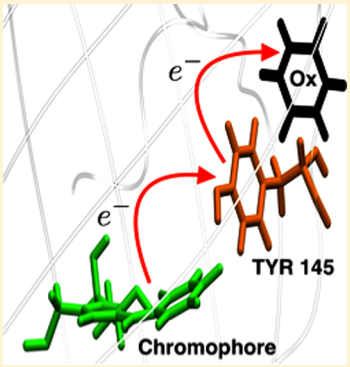

1. INTRODUCTION

Fluorescent proteins (FPs) from the green fluorescent protein family (GFP) enable detailed imaging of processes in live cells and even animals.[1,2] The GFP chromophore is formed autocatalytically upon protein folding and only requires ambient oxygen; thus, the FP sequence can be genetically encoded such that a fluorescent label is produced by an organism along with a protein it is tagging. Hundreds of FPs have been engineered to suit various imaging applications.[2] Among those, enhanced GFP (EGFP) and its yellow variant, EYFP, are considered standard general-purpose FPs.[3]

The GFP chromophore (Figure 1) features a conjugated π-system resembling cyanine dyes. The chromophore is buried inside a tight protein barrel that limits its range of motion and accessibility to solvent and other species (ions, oxygen, etc.). The protection of the barrel is essential for achieving high quantum yields (QY) and photostability, as compared to those of regular dyes.[1,4] For example, the GFP chromophore in aqueous solutions is nonfluorescent, whereas QY in EGFP is 0.6. Typical QY of bleaching in FPs is 10^{-4}–10^{-5}; it can be as low as 10^{-6} in buffered solutions when no oxidants are present.[5−8] The solution content can strongly affect photostability, even when the dissolved species are too large to penetrate the barrel. For example, oxidized flavines at ca. 1 mM decrease photostability of EGFP by up to an order of magnitude both *in vitro* and *in cellulo*.[9,10] Thus, significant changes in protein photobehavior may occur without the direct access to chromophore. Bleaching in some FPs is enhanced in the presence of oxygen and depends on oxygen accessibility to the chromophore.[11−14]

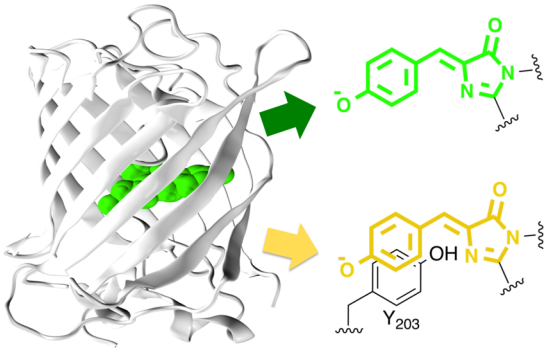

Figure 1. Structure of EGFP/EYFP. Left: β-barrel enclosing the chromophore. Right: EGFP and EYFP have the same anionic chromophore formed by cyclization and oxidation of the protein backbone at positions 65−67 (top). In YFPs, the chromophore is π-stacked with Tyr203 (bottom).

Received: January 13, 2016
Published: March 21, 2016

DOI: 10.1021/jacs.6b00092
J. Am. Chem. Soc. 2016, 138, 4807−4817

Multiple excited-state processes competing with fluorescence[4,15] are responsible for reduced optical output and bleaching. These include radiationless relaxation, formation of triplet states, photooxidation/photoreduction, and production of reactive oxygen species which can further react with the protein. Importantly, each of these processes can initiate a chemical transformation of the chromophore leading to temporary or permanent loss of fluorescence (i.e., reversible or irreversible bleaching) or change of color (photoconversion). Although in many situations these changes are regarded as parasitic processes, they are exploited in other techniques. For example, bleaching and photoswitching are utilized in super-resolution imaging,[2,4,16−18] methods based on fluorescence loss and recovery are used to trace protein dynamics, and photoconversions and photoswitching enable optical highlighting and timing of biochemical processes.[19,20]

In contrast to dyes, the photoinduced redox processes in FPs are not well-understood. These came into a spotlight in 2009, when it was discovered that FPs can be efficient light-induced electron donors.[21] Bogdanov et al. have reported that many FPs with an anionic GFP chromophore (such as one in Figure 1) undergo photoconversion from green to red form upon irradiation in the presence of oxidants. This process, dubbed oxidative redding, may be exploited in various applications.[2,20,22] Chemical steps leading to the red chromophore formation are initiated by photooxidation, photoinduced electron transfer (ET) from the chromophore to an external oxidant molecule.[21] Another type of photoconversion (based on the stabilization of the anionic form of the chromophore relative to the protonated neutral one) also involves a photoinduced redox process; photoinduced ET from nearby Glu to the chromophore is believed to be a gateway step leading to decarboxylation.[23,24] Recently, photoreduction of the chromophore was invoked to explain the formation of red-shifted transient species in red FPs.[25] Photoinduced ET from the anionic chromophores to O_2 may lead to superoxide formation, which might be responsible for phototoxicity.[26,27] Photoinduced ET coupled with proton transfer has been invoked in the proposed mechanism of bleaching in IrisFP.[28,29]

Oxidative redding was observed in various FPs that share the anionic GFP-like chromophore;[21] later, similar photoconversions were engineered in orange FPs in which the GFP-like chromophore is extended to include a conjugated acylimine tail.[30,31] Thus, redding appears to be a robust process characteristic of anionic chromophores that is not very sensitive to the details of the protein environment. No structural information about the red chromophore is available, although several hypotheses were put forward.[21,22,32]

The formation of the red form occurs on a second-to-minutes time scale[21] and is likely to entail significant chemical transformation, such as extension of the conjugated π-system or breaking of the covalent bonds. These chemical steps are initiated by photoinduced ET from the chromophore (Chro) to an external oxidant molecule. Thus, one can describe redding as an effectively two-step process (Scheme 1).

The rate-determining step is the second step involving slow chemical changes. The first step is fast because it is limited by the excited-state lifetime (nanoseconds). It is a gateway step: No redding can occur if there is no ET. The yield of this step provides an upper bound for the yield of the red form.

Here, we investigated three YFPs derived from *Aequorea victoria*: EYFP, Venus, and Citrin.[7,33,34] These YFPs have the same anionic chromophore as EGFP; the change of color is due to π-stacking of the chromophore with a nearby tyrosine residue (Tyr203, Figure 1). Surprisingly, we found that redding does not occur in these YFPs. However, in EYFP the redding can be turned on by halides, Cl^-, I^-, Br^-, and F^- (EYFP has a halide binding pocket and is used as a halide sensor).[33,35] This puzzling finding stimulated theoretical investigations and provided an opportunity to gain an insight into a mechanism of photoinduced ET in FPs. By using molecular dynamics (MD) and quantum-mechanics/molecular-mechanics (QM/MM) simulations, we computed Gibbs free energies and electronic couplings for various ET pathways. The simulations suggested that photoxidation of the chromophore proceeds predominantly by hopping mechanism via Tyr145 residue and that Tyr203 affects this major pathway by modulating the ET rate between the chromophore and Tyr145 and by acting as a trap site for ET. The effect on the rate is explained by electronic factors (changes in chromophore's oxidation potential due to π-stacking) and structural variations (changes in the Chro−Tyr145 distance). The theoretical predictions were validated by point mutations, which showed that replacing Tyr145 by less-efficient electron acceptors results in highly photostable FPs. These results represent the first step toward developing detailed mechanistic understanding of photoinduced ET in FPs and its role in bleaching and photostability.

Scheme 1. Steps Involved in the Oxidative Redding Process Leading to Final Red Form

$$Chro^- \xrightarrow{h\nu} Chro^{-*} \xrightarrow{fast,\ -1e} Chro^{\cdot} \xrightarrow{slow,\ chemistry} Red\ form$$

2. EXPERIMENTAL AND COMPUTATIONAL DETAILS

The experimental measurements were carried out as follows. His-tagged proteins were expressed in *Escherichia coli* and purified by a metal-affinity resin. The resin beads with immobilized proteins were placed into phosphate-buffered saline (PBS) with 0.5 mM potassium ferricyanide as an oxidant and illuminated with strong blue light using a fluorescence microscope. Changes of fluorescence in green/yellow and red channels were monitored during illumination. In addition, *in cellulo* measurements have been carried out.

2.1. Microscopy. For wide-field fluorescence microscopy, a Leica AF6000 LX imaging system with Photometrics CoolSNAP HQ CCD camera was used. Green and red fluorescence images were acquired using 63× 1.4NA oil-immersion objective and standard filter sets: GFP (excitation BP470/40, emission BP525/50) and TX2 (excitation BP560/40, emission BP645/75). For confocal microscopy, a Leica laser-scanning confocal inverted microscope DMIRE2 TCS SP2 with an 63× 1.4NA oil objective and 125 mW Ar laser was used. Live Human embryonic kidney 293 (HEK293T) cells expressing target proteins in cytoplasm were imaged and bleached using the following settings: 512 × 512 points, zoom 16 (15 × 15 mkm field of view), 488 nm laser intensity 5% (1.5 mkW) for detection and 100% (120 mkW) for bleaching, and fluorescence detection at 500−550 nm. Photobleaching and redding were monitored in time-lapse imaging in the green and red channels at low light intensity combined with exposures to blue light of maximum intensity (GFP filter set or 100% 488 nm laser). Images were acquired and quantified using Leica LAS AF and Leica Confocal software.

2.2. Protein Expression and Purification. EYFP, Venus, Citrine, and EGFP as well as EGFP-Y145L, EGFP-Y145F, EYFP-Y145L, and EYFP-Y145F mutants were cloned into the pQE30 vector (Qiagen) with a 6His tag at the N terminus, expressed in *E. coli* XL1 Blue strain (Invitrogen) and purified using TALON metal-affinity resin (Clontech). For mammalian cell expression, EGFP-N1 vector backbone (Clontech) was used. EYFP, its mutants, and EGFP mutants were cloned into EGFP-N1 instead of EGFP. HEK293T cells

DOI: 10.1021/jacs.6b00092
J. Am. Chem. Soc. 2016, 138, 4807−4817

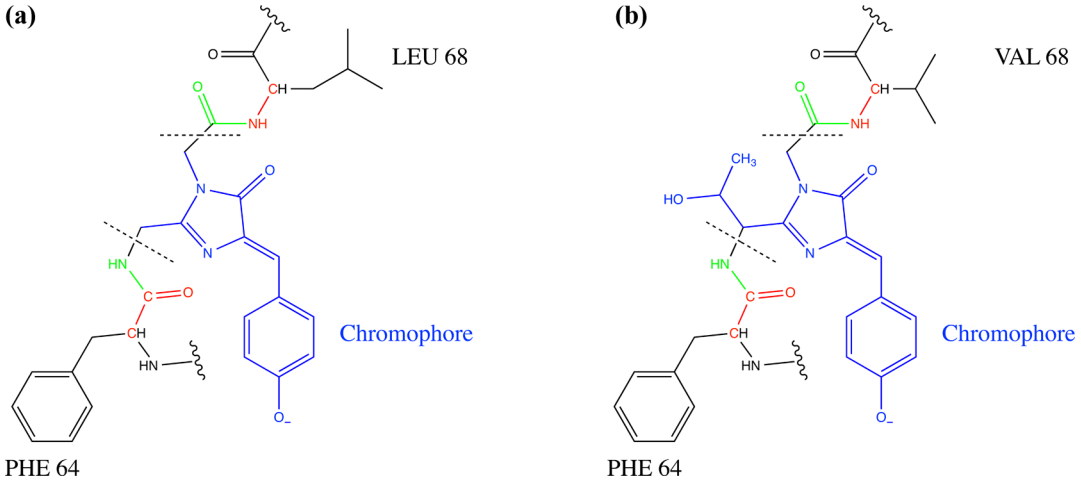

Figure 2. QM/MM schemes for (a) EYFP and (b) EGFP used in the calculations of the ionization energies of the chromophore. The black dotted lines denote the boundary between the QM (blue) and MM parts. The MM part, in which point charges were set to zero, is denoted by green and red (note that green atoms are part of the chromophore).

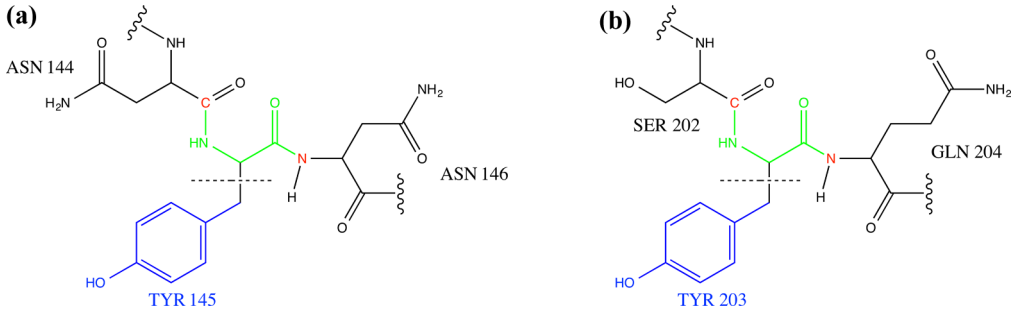

Figure 3. QM/MM scheme used in the calculations of electron attachment energies of tyrosines: (a) Tyr145 and (b) Tyr203. The black dotted lines denote the boundary between the QM (blue) and MM parts. The MM part in which point charges were set to zero is denoted by green and red (note that green atoms are part of tyrosine).

(ATCC) were transfected with the above listed constructs to obtain transient protein expression.

2.3. Mammalian Cell Culture and Transfection. The HEK293T cell line was used. Cells were transfected with EGFP-N1 (Clontech) and derived plasmids (section 2.2) using FuGene6 reagent (Promega) and growth in DMEM (Paneco) containing 10% FBS (Sigma). Live cells in the same medium were imaged 36 h after transfection using the Leica AF6000 LX fluorescence microscope and Leica SP2 confocal microscope at room temperature.

2.4. Site-Directed Mutagenesis. The EGFP Y145L, EGFP Y145F, EYFP Y145L, and EYFP Y145F mutants were generated using overlap-extension PCR technique with the following oligonucleotide set containing the appropriate substitutions: forward 5′-ATGCGGATCCATGGTGAGCAAGGGCGAG-3′, reverse 5′-ATGCAAGCTTTTACTTGTACAGCTCGTC-3′ and forward 5′-GAGTACAACTTCAACAGCCAC-3′ and reverse 5′-GTGGCTGTTGAAGTTGTACTC-3′ for EYFP and EGFP Y145F; forward 5′-ATGCGGATCCATGGTGAGCAAGGGCGAG-3′, reverse 5′-ATGCAAGCTTTTACTTGTACAGCTCGTC-3′ and forward 5′-GAGTACAACCTGAACAGCCAC-3′, reverse 5′-GTGGCTGTTCAGGTTGTACTC-3′ for EYFP and EGFP Y145L. For bacterial expression, a PCR-amplified *Bam*HI/*Hin*dIII fragment encoding an FP variant was cloned into the pQE30 vector (Qiagen). For mammalian expression, a PCR-amplified (with 5′-CAGTACCGGTCGCCACCATGGTGAGCAAGGGCGAGGAGCTG-3′ and 5′-GATCGCGGCCGCTCACTTGTACAGCTCGTCCATGCCG-3′) AgeI/NotI fragment encoding an FP variant was cloned into EGFP-N1 vector (Clontech) instead the original EGFP gene.

2.5. Computational. Protein Databank structures 1F09 and 1F0B[33] were used to represent YFP with and without halide. For GFP, the 1EMA structure was used.[36] The details of the model system setup and protonation states of the key residues around the chromophore are given in the Supporting Information. To identify possible binding sites for an outside oxidant, we carried out docking calculations using *AutoDock*.[37] These calculations were followed by the MD simulations (10 ns). We carried out semiempirical calculations of tunneling probabilities between the chromophore and various possible electron acceptors using the *Pathways* model[38] in which the tunneling probability between specified donor and acceptor is computed as a product of tunneling probabilities via all possible pathways. The model considers tunneling via covalent bonds, hydrogen bonds, and through space. The tunneling through the covalent bonds is assigned the highest probability, followed by tunneling through hydrogen bonds and through space. Thus, the *Pathways* model accounts for the distances and the connectivity (covalent and hydrogen bonds) between the donor and acceptor moieties.

To evaluate the feasibility of various mechanisms, we carried out detailed calculations of the rates of ET between different sites using the Marcus rate expression:[39,40]

$$k_{ET} = \frac{2\pi}{\hbar}|H_{DA}|^2 \frac{1}{\sqrt{4\pi\lambda k_B T}} \exp\left\{-\frac{(\Delta G + \lambda)^2}{4\lambda k_B T}\right\} \quad (1)$$

where ΔG, λ, and H_{DA} are the free energy change, reorganization energy, and coupling between the electronic states involved in ET. Relevant free energies and electronic couplings were computed using QM/MM. Thermodynamic averaging was carried out using Warshel's linear response approximation.[41] In this approach, ΔG and λ for the oxidation process are computed as

DOI: 10.1021/jacs.6b00092
J. Am. Chem. Soc. 2016, 138, 4807−4817

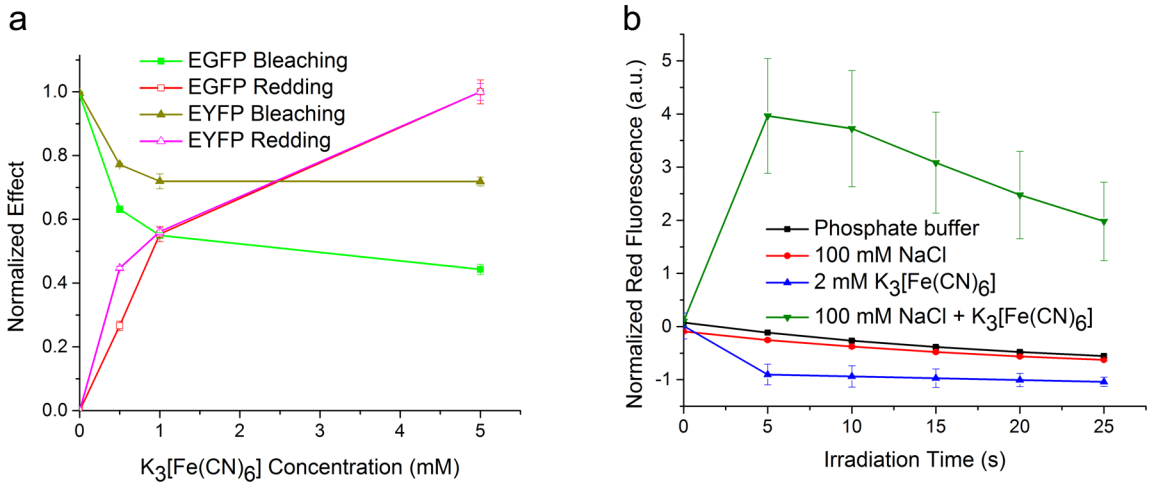

Figure 4. EGFP and EYFP oxidative photoactivation. (a) Effect of potassium ferricyanide concentration on the main (green/yellow) fluorescent state bleaching (green full squares/yellow full triangles) and the red fluorescence increase (red open squares/magenta open triangles) in the oxidative redding of immobilized EGFP and EYFP. After one activating irradiation cycle with GFP filter set, the remaining green fluorescence (normalized according to initial value) and originating red fluorescence (normalized according to maximal value) were measured and shown in the graph. (b) Red fluorescence appearance in EYFP during irradiation. Immobilized EYFP was irradiated with arc-lamp (GFP filter set, 0.6 W/cm^2) in phosphate buffer (black squares), in the presence of oxidant (blue triangles), in the presence of sodium chloride (red circles), and in the presence of both oxidant and chloride (green triangles). Redding efficiency is normalized according to initial yellow fluorescence. Each data point is an average of three independent experiments. Error bars, s.d.

$$\Delta G_{ox} = \frac{1}{2}(\langle E_O - E_R\rangle_R + \langle E_O - E_R\rangle_O) \quad (2)$$

$$\lambda_{ox} = \frac{1}{2}(\langle E_O - E_R\rangle_R - \langle E_O - E_R\rangle_O) \quad (3)$$

where E_O and E_R are electronic energies of the oxidized and reduced states of the chromophore (or tyrosine) and the brackets indicate thermodynamic averaging (subscripts *R* and *O* correspond to the averaging on the reduced and oxidized states). We used the following protocol to compute these quantities. First, we carried out MD for the initial (Chro$^-$) and oxidized (Chro$^{\cdot}$) states of the protein to generate equilibrium sampling (for tyrosine, the two states corresponded to Tyr and Tyr^{-}). We then followed with the QM/MM calculations of E_O−E_R on both states. To calculate the energetics for ET between the chromophore and selected residues, instead of E_O−E_R we computed the energy differences between the initial (Chro$^-$···ResX) and charge-transfer (Chro···ResX^{-}) states.

Figures 2 and 3 show QM/MM schemes used in the calculations. In calculations of the ionization energy of the chromophore, the QM system contained the chromophore. For computing electron attachment energies of tyrosines (Tyr145 or Tyr203), the QM system contained the respective residues. In CDFT-CI calculations, the QM system contained both the chromophore and the accepting tyrosine moiety.

Following protocols validated in our previous calculations of the redox potentials, in QM/MM calculations[42,43] we used the ωB97X-D functional, which includes exact long-range exchange and dispersion correction.[44,45] The detailed protocol is described in the Supporting Information.

To understand the trends in the computed ET rates, we analyzed relevant structural parameters along equilibrium trajectories for various systems. MD simulations were performed using NAMD.[46] Electronic structure and QM/MM calculations were carried out using Q-CHEM.[47] CDFT-CI was used for calculations of couplings.[48] CHARMM27 parameters for standard protein residues[49] and the parameters derived by Reuter et al. for the anionic GFP chromophore were used in the MD calculations.[50] The parameters for the oxidized/reduced residues were derived from additional quantum mechanical calculations, as described in the Supporting Information.

3. RESULTS AND DISCUSSION

Figure 4a shows the normalized yields of bleaching (green/yellow form disappearance) and redding (red form appearance) as a function of the oxidant concentration for EGFP and EYFP (in the presence of chloride). When chloride is present, EYFP behaves similarly to EGFP. As one can see, the bleaching of the green form and the yield of the red form depend strongly on the concentration of the oxidant. Thus, under these conditions, the bleaching is mainly due to photooxidation. Therefore, the disappearance of the green/yellow form, which describes bleaching kinetics, can be loosely correlated with the ET step from Scheme 1; as shown previously, one-electron oxidation leads to the formation of radical with strongly blue-shifted absorption.[32] The rise of the red signal is related to the second step, the red chromophore formation. The upper bound for the total yield of the red form is given by the yield of the one-electron oxidized form of the chromophore, a precursor of the red form. As shown below, mutations and variations in experimental conditions affect the two signals differently (e.g., some strongly affect bleaching kinetics, whereas others have no effect on bleaching but lead to changes in the red form buildup).

As mentioned in the Introduction, this study was motivated by a drastically different behavior of YFPs relative to that of EGFP. When no halides are present, no red signal is observed in any of the three YFPs. It is known that EYFP's fluorescence is sensitive to Cl$^-$, and Venus and Citrin lack this sensitivity.[7,33,34,51] Thus, we tested the influence of Cl$^-$ on EYFP's redding. Indeed, we found that EYFP undergoes yellow-to-red photoconversion only in the presence of chloride (Figure 4b). Because Cl$^-$ quenches EYFP's fluorescence as a result of electrostatic stimulation of chromophore protonation,[33,51] we also tested photoconversion of EYFP at different pH. In the absence of Cl$^-$, EYFP redding was not detected even at low pH leading to complete chromophore protonation (Figure S3). Thus, we concluded that the effect of Cl$^-$ is not related to chromophore's protonation state. Next, we tested the

DOI: 10.1021/jacs.6b00092
J. Am. Chem. Soc. 2016, 138, 4807−4817

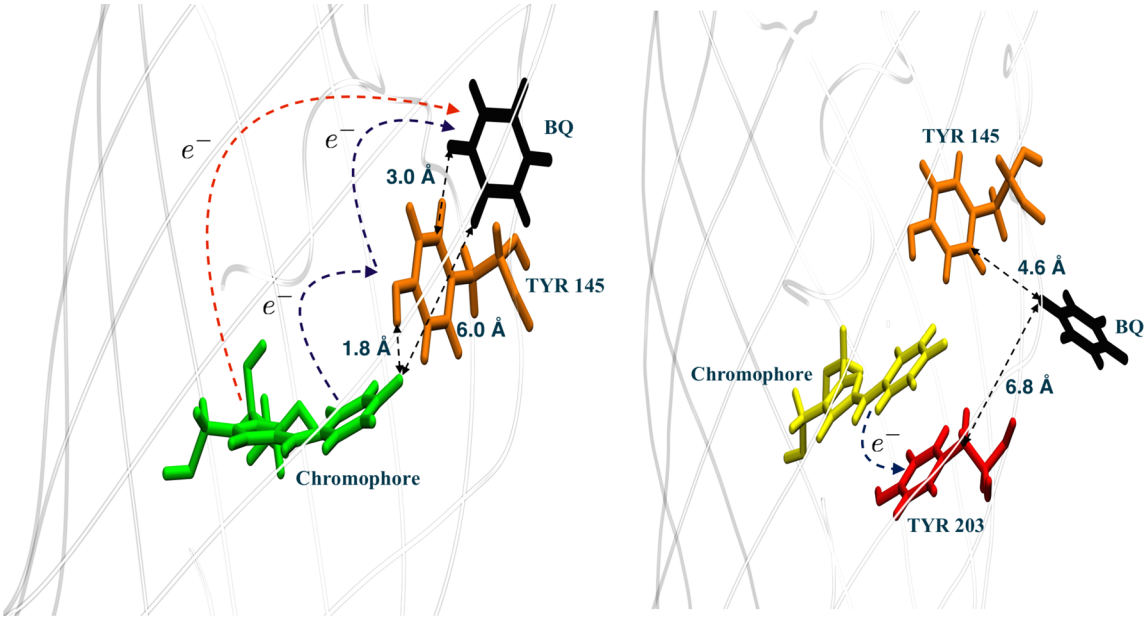

Figure 5. Mechanism of photoinduced ET in FPs. An oxidant molecule (represented by *para*-benzoquinone, BQ) docked to EGFP (left) and EYFP (right) and the relevant distances. The direct tunneling and two-step hopping (via Tyr145) mechanisms for ET are shown by dashed arrows.

influence of different halide ions on EYFP's redding and found that efficiency of photoconversion decreases in the series $F^- > Cl^- > Br^- > I^-$; thus, it can be correlated with the size of the halide, as shown in Figures S1 and S2.

To understand the different behavior of YFPs relative to EGFP, we turn to the analysis of possible mechanisms of photoinduced ET, drawing from the extensive studies of ET in proteins.[52−56] ET in proteins can proceed through large distances, up to 20 Å; rates between 10^2−10^8 s^{-1} have been observed.[52] The rates decay exponentially with the donor−acceptor distance. In many redox-active proteins, the ET proceeds between well-defined redox sites; in such systems the discussion of the mechanism focuses on identifying dominant pathways for ET (or the absence of thereof) and discrimination between direct ET (one-step transport via coherent tunneling or flickering resonance) and hopping (multistep ET via intermediate electron acceptors) mechanisms. One-step ET can proceed through space (if the donor and acceptor residues are sufficiently close) or can be mediated by covalent or hydrogen bonds (bridge-mediated superexchange). Multistep hopping entails transient localization of charge carriers, i.e., formation of reduced or oxidized intermediates along the ET pathway.

In the case of FPs, the location of the electron-accepting oxidant molecule is not known. The distance between the chromophore and the closest solvent-accessible surface sites is about 8−10 Å. Thus, the oxidant cannot form a close contact with the chromophore. To identify an access point which is most favorable for ET, we investigated possible docking sites with an aim to identify those corresponding to the shortest chromophore−oxidant distances. Note that efficient redding was observed[21] using a variety of oxidant molecules including rather bulky ones such as cytochrome c that cannot penetrate the tight GFP barrel. In our simulations, we used *para*-benzoquinone, BQ, as a model oxidant. Docking calculations revealed several docking sites on the surface of the barrel. Among those, we identified a cluster of structures corresponding to the shortest chromophore−BQ distance; these structures for EGFP and EYFP are shown in Figure 5. To verify the results of the docking simulations, we carried out MD simulations for the docked structure with the shortest chromophore−BQ distance. We observed that the distance between Tyr145 and BQ stays mostly within 3.9−5.4 Å throughout a 10 ns long MD trajectory. The detailed discussion of the docking and MD simulations is given in the Supporting Information.

The distance between Chro and BQ in these structures is about 6 Å, which is sufficiently short to consider direct tunneling. We also considered a possibility of ET by a hopping mechanism via residues with aromatic groups such as tryptophan, tyrosine, phenylalanine, or histidine. A similar mechanism involving aromatic residues serving as "stepping stones" for charge transfer in respiratory complex I has been introduced to explain the experimentally observed fast rates for ET.[57] On the basis of their electron affinities, we identified tryptophan and tyrosine as the most likely acceptors. We analyzed the structures of EGFP and EYFP identifying those residues in the vicinity of the chromophore. In addition to structural analysis, we also performed semiempirical calculations using the *Pathways* model[38] which allows one to compare tunneling probabilities (T_{DA}) between different sites and to identify the residues that mediate ET. These calculations identified Tyr145 as the most probable electron acceptor both in EYFP and EGFP (T_{DA} = 1.7 × 10^{-2} and 1.9 × 10^{-2}, respectively). In EYFP, the tunneling probability to Tyr203 was of the same magnitude as that for Tyr145 (2.3 × 10^{-2}). For other tyrosines, the computed tunneling probabilities were at least an order of magnitude lower. T_{DA} for the direct ET (from Chro to BQ) was 4.6 × 10^{-3} (in EGFP); this pathway is mediated by Tyr145.

Thus, on the basis of docking and tunneling calculations, we put forward two mechanistic hypotheses (Figure 5): (i) direct tunneling to the outside oxidant (docked in the vicinity of Tyr145 and mediated by it) and (ii) two-step hopping mechanism in which the electron is first transferred to Tyr145, forming a transient radical anion, and then is picked up by the oxidant. Other competing channels may be

DOI: 10.1021/jacs.6b00092
J. Am. Chem. Soc. 2016, 138, 4807−4817

operational, e.g, in EYFP, ET to Tyr203 might occur; Phe165 or Tyr92 may also be involved. Importantly, Tyr145 is much closer to the surface than Tyr203. Thus based on the docking and *Pathways* calculations, Tyr145 might be an efficient intermediate electron acceptor mediating the ET to an outside oxidant, whereas Tyr203 (or other residues buried deeply inside the barrel) are inaccessible to the oxidants and are likely to be trap sites leading to either permanent bleaching (via chemical reactions of the resulting radical) or quenching (by back ET to the chromophore).

To evaluate the feasibility of these mechanisms, we performed detailed calculations of the rates of ET between different sites using the Marcus rate expression,[40] eq 1, and QM/MM calculations of relevant free energies and electronic couplings using high-level electronic structure methods and Warshel's linear response approximation[41] for thermodynamic averaging (see Supporting Information for details). We then analyzed the differences between EGFP, EYFP with and without chloride, and mutants. To make quantitative comparisons between different systems and to compare with the experiment, we focus on evaluating QY of the precursor of the red form, the product of one-electron oxidation of the chromophore.

For the direct tunneling mechanism, QY of bleaching is determined by the competition between the two channels: radiative or/and radiationless decay of the excited state (characterized by the combined rate, r_f) restoring the ground-state chromophore and ET (r_{et}). The QY of the red-form precursor is then:

$$Y_r = \frac{r_{et}}{r_{et} + r_f} \approx \frac{r_{et}}{r_f} \tag{4}$$

This expression allows us to estimate an anticipated order of magnitude for ET rates. Using typical fluorescence lifetime (nanoseconds, $r_f \approx 10^9\ s^{-1}$) and a typical QY of bleaching[4,7,8] $Y_{bl} \approx 10^{-5}$, the estimated ET rate is then $10^4\ s^{-1}$ (slower rates will result in lower bleaching yields). Because the yield of the precursor can be higher than that of the bleached form, this estimate provides a lower bound to the ET rate.

The kinetic model for the hopping mechanism is shown in Figure 6. It comprises five states: ground-state and electronically excited chromophore, oxidized chromophore (red-form precursor), and two intermediate states in which the chromophore is oxidized and the electron resides on one of the protein residues (Tyr145 or a trap site, TyrX). r_2, the rate of ET between Tyr145 and an outside oxidant, is expected to be very fast, as this is an exothermic step. The upper bound is given by the diffusion-limited rate, $r_2 = 2 \times 10^{10}\ s^{-1}$. We consider the following mechanism for photoinduced ET via hopping. We assume that in EGFP, there is a direct ET pathway from $Chro^{-}$* to Tyr145, the rate is given by r_1. Once the electron reaches Tyr145, it can either go back (r_{-1} and r_3) restoring the anionic chromophore, or initiate some chemistry (potentially leading to bleaching), or irreversibly tunnel out (r_2, fast), to an outside oxidant forming a red-form precursor. There is a competing channel, r_4, to ResX; this channel can lead to either permanent bleaching (r_b) or to restoring the chromophore (r_{-4} and r_5). In EYFP, ResX ≡ Tyr203; in EGFP, ResX might be Tyr92 or another acceptor. As illustrated by the *Pathways* model and docking calculations, Tyr203 is buried inside the barrel and the pathway for ET from Tyr203 to Tyr145 involves the chromophore, thus increasing the probability of quenching. Therefore, r_6 is expected to be slow, making Tyr203 a dead-end for photooxidation.

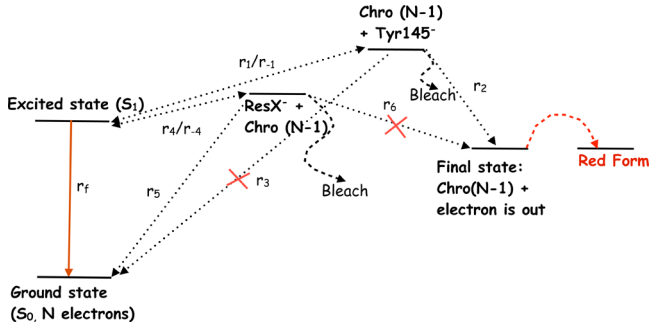

Figure 6. Kinetic model of photoinduced ET via hopping mechanism. The excited state can decay to the ground state, either radiatively or nonradiatively. This channel is characterized by r_f, which is inversely proportional to the excited-state lifetime ($r_f \approx 10^9\ s^{-1}$). Alternatively, the excited state can decay via ET from the chromophore to either Tyr145 or another acceptor, ResX, which could be Tyr203 in EYFP. ET to Tyr145 or ResX results in anion-radical (e.g., $Tyr^{-\cdot}$) formation that can lead to permanent bleaching (r_b). ET to Tyr145 can also lead to ET to an outside oxidant (r_2) forming a precursor of the red form. The observed bleaching is the sum of the yields of the red form precursor and of permanently bleached states. Based on our rates calculations, r_3 and r_6 are slow; r_5 is slow for Tyr203.

The detailed analysis of this kinetic model is given in the Supporting Information; the main result is

$$Y_r \approx \frac{r_1}{r_f\left(1 + \frac{r_b}{r_2}\right)} \approx \frac{r_1}{r_f} \tag{5}$$

$$Y_{totb} \approx \left(\frac{r_1}{r_f} + \frac{r_4}{r_f}\right)\left(1 + \frac{r_b}{r_2}\right) \approx \frac{r_1}{r_f} + \frac{r_4}{r_f} \tag{6}$$

We note that the $\frac{r_b}{r_2}$ term is likely to be small because r_2 is expected to be much faster than the rate of chemical reactions leading to permanent bleaching and is, therefore, neglected in the present analysis. Thus, the trend in the yield of red form is dominated by the $\frac{r_1}{r_f}$ ratio; as in the direct tunneling mechanism, the lower bound for r_1 is $10^4\ s^{-1}$. The total yield of the bleached form, Y_{totb} is roughly equal the sum of yields of the red-form precursor and a permanently bleached form produced via a competing channel (ET to ResX). For this channel to have a noticeable effect on the yield, rate r_4 should be comparable to (or larger than) r_1.

In both mechanisms (direct or hopping), Tyr145 may play a role, either as a mediating residue or as a transient electron acceptor; thus, in the calculations below we consider the effect of mutation of this residue on the computed rates and yields.

Table 1 shows the key quantities related to the redox properties of FPs in the ground and electronically excited states. For the oxidation process to be thermodynamically favorable, $\Delta G_{ox}(Chro) + \Delta G_{red}(OX)$ should be negative. The original GFP redding study[21] reported that EGFP can be oxidized by various oxidizing agents with E^0 up to −0.114 V relative to the standard hydrogen electrode (SHE), which translates into $\Delta G_{red} = -4.167$ eV at pH = 0, using $\Delta G(SHE) = 4.281$ eV.[58] Thus, the computed energetics is consistent with estimated ΔG_{red}: Oxidation of the ground-state chromophore is not thermodynamically favorable; however, it becomes possible upon electronic excitation. We also observe that EYFP is more

DOI: 10.1021/jacs.6b00092
J. Am. Chem. Soc. 2016, 138, 4807−4817

Table 1. Redox Properties of the Ground-State and Electronically Excited Chromophores of EGFP, EGFP-Y145L, EYFP, and Halide-Bound EYFP at T = 298 K

system	ΔG_{ox}^{gs} (eV)	λ_{ox} (eV)	ΔG_{ox}^{ex} (eV)
EGFP	4.551	1.599	2.111
EYFP	4.697	1.400	2.347
EYFP + Cl^-	4.274	1.686	1.924
EGFP-Y145L	4.548	1.528	2.108

difficult to oxidize relative to EGFP, whereas chloride binding reduces ΔG_{ox}. This is due to π-stacking with Tyr203, which increases ionization energy. The effect of chloride binding is two-fold: it upsets π-stacking and also decreases the ionization energy due to electrostatic interactions. The Y145L mutation does not affect ΔG_{ox} of the chromophore. Using the data from Table 1 and estimated ΔG_{red} and λ_{red} for BQ, we can estimate the rates (and Y_r) for the direct tunneling mechanism; these data are presented in Table S17. The main result of these calculations is that despite the variations in ΔG_{ox} the direct ET mechanism predicts similar rates in EGFP, EYFP, and chloride-bound EYFP. Thus, it does not explain the experimental findings. This direct tunneling model also predicts that the Y145L mutation will have no effect on the ET rate because the free energy of oxidation of the chromophore is not affected, as can be seen from Table 1.

The Gibbs free energies, electronic couplings, and the rates for ET via hopping mechanism are collected in Table 2 (more details are given in the Supporting Information).

Table 2. Relevant Gibbs Free Energy Differences, Reorganization Energies, Couplings, and Marcus Rates for ET at 298 K[a]

system	final state	ΔG_{CT}^{ex}	λ_{CT}	$\lvert H_{DA}\rvert^2$	r_1 or r_4
EGFP		0.452	0.846	0.214	1.5×10^7
EYFP	CT 145	0.783	0.704	0.141	1.5×10^2
EYFP+Cl^-		0.561	0.787	0.590	2.0×10^6
EYFP		0.564	0.287	0.180	1.2×10^5
EYFP-Y145L	CT 203	0.636	0.394	0.097	1.1×10^4
EYFP+Cl^-		0.857	0.235	0.067	8.4×10^{-7}

[a]Energy and coupling values are given in eV and eV^2, respectively, and the rate constants are in s^{-1}.

The computed rates show that ET to Tyr145 is strongly affected by π-stacking and by halide binding. π-stacking completely shuts down the main channel and opens up another ET channel, to Tyr203. The halide binding opens up the main channel and shuts down ET to Tyr203. The computed Y_r are Y_r(EGFP) = 1.5%, Y_r(EYFP) = 2×10^{-5}%, and Y_r(EYFP+Cl^-) = 0.2%. We also performed calculations using a strong coupling regime (Supporting Information). The computed rates are slower (giving rise to lower QY), but the main trend remains the same. Thus, the hopping model reproduces the observed differences between the three proteins. We note that the computed rate for ET to Tyr203 in EYFP is sufficiently large to have a noticeable effect on the total yield of bleaching and that chloride binding completely shuts down this competing channel. Other residues, such as Tyr92 or Phe165 may, in principle, contribute to this channel (their possible roles will be investigated in future study). The calculations suggest that the observed bleaching in EYFP without halide is due to permanent bleaching via ET to Tyr203, whereas in the presence of halide, most of the bleaching results from forming the red-form precursor.

To understand the differences in the computed ET rates in EGFP, EYFP, and chloride-bound EYFP, we analyzed relevant structural parameters along the equilibrium MD trajectories. We focus on the distance between the chromophore and Tyr145 and between the chromophore and Tyr203 (in EYFP). Table 3 summarizes the results. d_1 is defined as the distance between the oxygen of chromophore and Tyr145 phenolic oxygen; the variations in this distance are expected to modulate the energetics and couplings defining r_1. To quantify the π-stacking between the chromophore and Tyr203, we computed the distances between the edges of the respective aromatic rings; these are denoted d_2 and d_3. The definitions of these structural parameters are shown in Figure 7. The distance between the two phenolic rings is given by $D = \frac{d_2 + d_3}{2}$, and the deviation from a perfectly parallel arrangement is given by $\Delta = |d_2 - d_3|$. As one can see, d_1 is about 1.2 Å longer in EYFP than in EGFP, but it shrinks upon chloride binding. Further analysis of the trajectories reveals that in EYFP there are two interconverting hydrogen-bond patterns: one in which there is a hydrogen bond between Tyr145 and the chromophore (in this structure, the relative orientation of Tyr145 and the chromophore is similar to EGFP and d_1 is small) and one in which Tyr145 moves away and forms a hydrogen bond with His169 (Figure S21). In the course of 12 ns equilibrium dynamics, the first structure is populated ~63% of the time (Figure S23). The presence of the two structures is responsible for the larger average value and large standard deviation of d_1 (Table 3). Chloride binding suppresses the second structure, which leads to shorter d_1; it also affects π-stacking. As one can see from Table 3, in EYFP the phenolic rings of the chromophore and Tyr203 are closer (shorter D) and more parallel (smaller Δ) than in chloride-bound EYFP. As

Table 3. Average Values of Relevant Structural Parameters for EGFP, EYFP, and EYFP+Cl^-[a]

system	d_1 (Å)	D (Å)	Δ (Å)
EGFP	3.77 (0.46)		
EYFP	5.03 (1.28)	3.97	0.25
EYFP+Cl^-	2.89 (0.25)	4.18	0.43

[a]The standard deviations are shown in parentheses. See Figure 7 for definition of structural parameters.

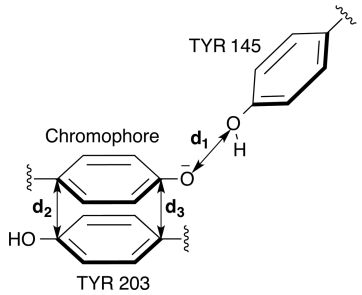

Figure 7. Relevant structural parameters. The distance between the phenolic oxygens of the chromophore and Tyr145 (d_1) affects the main ET channel (r_1). The extent of π-stacking can be quantified by $D \equiv \frac{d_2 + d_3}{2}$ and $\Delta \equiv |d_2 - d_3|$.

DOI: 10.1021/jacs.6b00092
J. Am. Chem. Soc. 2016, 138, 4807−4817

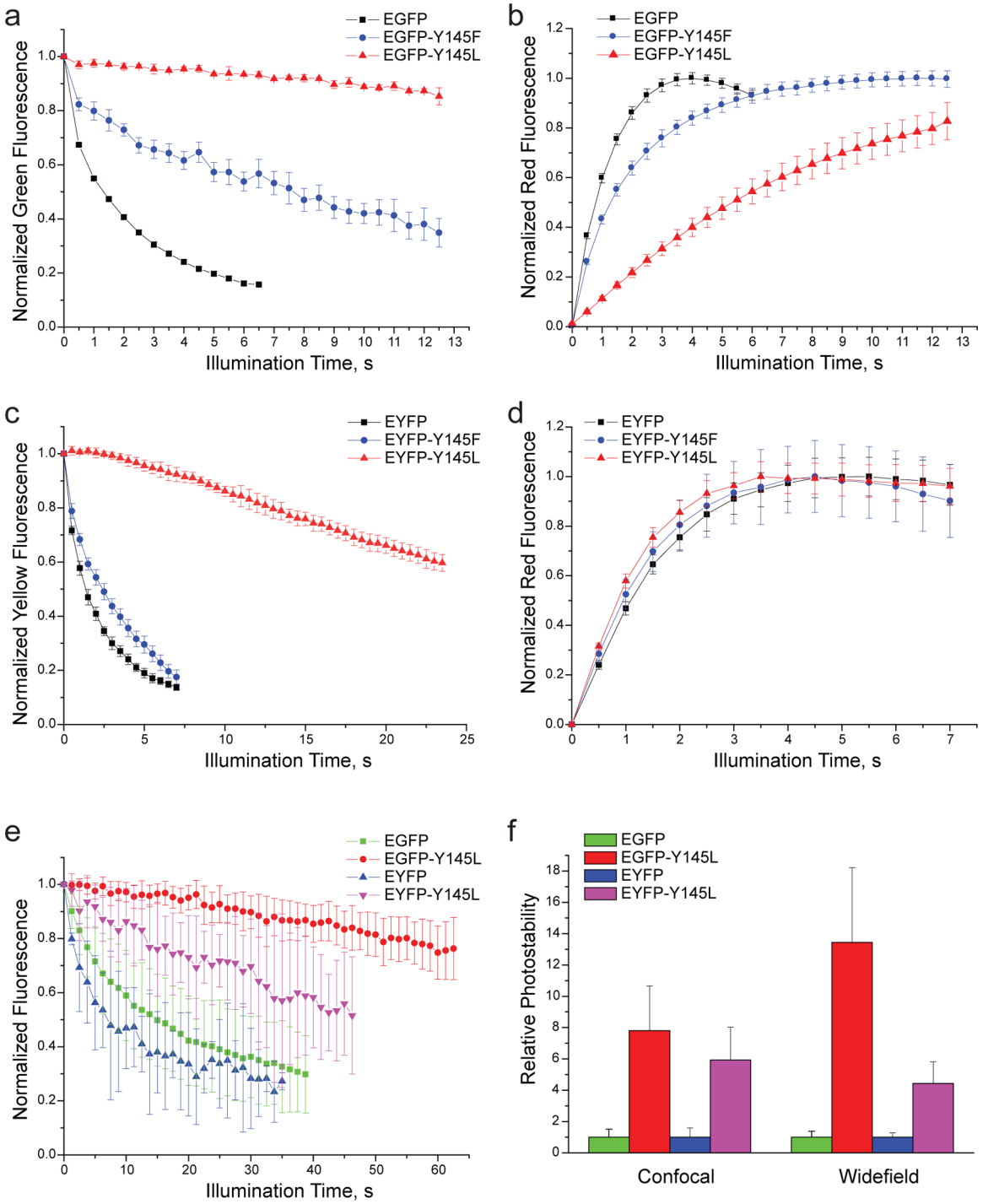

Figure 8. Bleaching and redding kinetics in the EGFP and EYFP mutants. (a–d) Photoconversion of immobilized proteins *in vitro* in PBS in the presence of 0.5 mM potassium ferricyanide. (PBS contains potassium chloride.) Graphs show the main form bleaching (a and c) and simultaneous appearance of red fluorescence (b and d) in EGFP, EGFP-Y145L, and EGFP-Y145F (a and b) and EYFP, EYFP-Y145L, and EYFP-Y145F (c and d). Green/yellow and red fluorescence intensities were background-subtracted and normalized to the maximum values. Standard deviation values (n = 15–20 measurements in a representative experiment out of five independent experiments) are shown. (e) Bleaching of EGFP, EGFP-Y145L, EYFP, and EYFP-Y145L in live HEK293 cells induced by 488 nm laser in a confocal microscope. (f) Increase of photostability (time to half-bleaching) of the EGFP-Y145L and EYFP-Y145L mutants compared to that of EGFP and EYFP, respectively, under confocal and widefield microscopy of live HEK293 cells. Standard deviation values for 50–60 cells in three independent experiments are shown.

illustrated in Figure S18, π-stacking controls the delocalization of electronic density between the chromophore and Tyr203, which, in turn controls electronic couplings and affects orbital energies. Thus, on the basis of the structural analysis, we conclude that the rate of ET between the chromophore and Tyr145 (r_1) is suppressed in EYFP because of the (i) increase of the chromophore's electron detachment energy due to π-stacking with Tyr203 and (ii) the presence of the conformation in which the hydrogen bond between the chromophore and Tyr145 is broken. Chloride binding suppresses the structural

DOI: 10.1021/jacs.6b00092
J. Am. Chem. Soc. 2016, 138, 4807–4817

fluctuations, which leads to shorter Chro-Tyr145 distances and increased r_1. Chloride binding also distorts π-stacking of the chromophore with Tyr203, which shuts down this competing ET channel (r_4).

Within the hopping model, the magnitude of r_1 determines the yield (eq 5). Thus, the model predicts that the photooxidation efficiency can be controlled by the mutations of residue 145. The effect of mutation of Tyr145 to phenylalanine and leucine is expected to increase ΔG_{CT} by about 0.07 eV or more. This would result in r_1 decrease by a factor of 8−10 in EGFP and EYFP+Cl^- reducing the yields proportionally. For the Y145F mutant, we estimated changes in free energies and couplings from snapshots of MD simulations (Supporting Information) and found that the rate for ET drops by at least a factor of 2, with the main effect being the decrease in the coupling because of the lack of hydrogen bond with the chromophore. For the EYFP-Y145L mutant, we also computed the rate for ET to Tyr203 (r_4). The mutation results in the one order of magnitude drop of r_4 (Table 2), which suggests the increased photostability of the EYFP-Y145L mutant at nonoxidative conditions, i.e., without halide binding and in the absence of oxidants.

As one can see from Table 2, the ET to Tyr145 is endothermic and is expected to slow down at low temperature. This trend may be partially offset by the increased electronic couplings and small increase in fluorescence lifetime. The calculations predict a moderate drop in r_1 and, consequently, in Y_r, e.g., in EGFP $Y_r(273)/Y_r(298) = 0.23$.

To test the theoretical prediction of the role of Tyr145 as an intermediate electron acceptor in the two-step hopping mechanism, we conducted mutagenesis studies. The mutants of EGFP and EYFP were constructed by mutating residue 145 to phenylalanine and leucine. As illustrated in Figure 8, mutating Tyr145 to a less favorable electron acceptor led to a significantly reduced bleaching. The effect was stronger for leucine; both the EGFP-Y145L and EYFP-Y145L mutants were very photostable (Figure 8a,c). Although mutants with Leu145 have decreased extinction coefficients (Table S1), 80- and 25-fold increased photostabilities of EGFP-Y145L and EYFP-Y145L can not be attributed solely to the 3- to 5-fold decrease of their extinction coefficients (compared to EGFP and EYFP, respectively). As reported in a recent study,[59] the fluorescence QY and lifetimes in Y145L and Y145F mutants are very similar to those in EYFP. Thus, strikingly different photostability can be attributed to the ET channel and not to the changes in radiative and radiationless population decay of the excited state. In the EGFP mutants, the rate of red form appearance was also suppressed (Figure 8b). At the same time, mutants of EYFP showed no significant changes of the redding rate (Figure 8d), suggesting that Y145L/F mutations affect both steps in Scheme 1.

To test whether the increased photostability of the mutants persists at the conditions relevant to imaging studies, we conducted *in cellulo* measurements. As illustrated in Figure 8e,f, the EGFP-Y145L and EYFP-Y145L mutants expressed in mammalian cells demonstrated several fold increased photostabilities relative to the respective parental proteins in both laser scanning confocal and widefield fluorescence microscopy.

As discussed above, the hopping model via Tyr145 predicts reduced rates of photooxidation at low temperature. To verify this prediction, we compared oxidative photoconversion of EGFP *in vitro* in the presence of 0.5 mM potassium ferricyanide at 273, 295, and 310 K (Figure S4). In agreement with theory, EGFP's bleaching and redding rates are slightly enhanced at elevated temperature.

Obviously, photostability represents one of the most important characteristics of a fluorescent protein. Unfortunately, mechanisms of FP photobleaching are poorly understood. Some amino acid substitutions (mainly found by chance) were shown to strongly enhance the photostability of FPs, especially those with low photostability. For example, photostability of EBFP was dramatically (two orders of magnitude) increased by V150I plus V224R mutations.[60,61] Single-substitution S158T (corresponding to position 165 in GFP) strongly improved photostability of TagRFP.[62] In chloride-sensitive variant of yellow fluorescent protein ClsM, mutation S205V substantially suppressed photobleaching.[63] A common feature of these mutants is the insertion of bulkier residues. It results in a decrease or full elimination of fast initial phase of bleaching, which is thought to represent cis−trans chromophore isomerization and/or protonation−deprotonation events.[64−66] Also, a possible reason for photostability enhancement is lowering the accessibility of the chromophore to molecular oxygen by bulky residues. There are a few crystallographic studies directly demonstrating chromophore destruction[67−69] or oxidation of chromophore-adjacent Met and Cys residues[29] in photobleached FPs. The latter possibly explains a key role of the mutation M163Q (position 167 in GFP) in a high photostability of mCherry.[62]

In contrast to the previous investigations of photostability, our study provides concrete mechanistic suggestions about bleaching via photoinduced ET and therefore furnishes a design principle for rational engineering of more photostable FPs. We identified Tyr145 as a key residue controlling ET and demonstrated that its substitution by less effective electron acceptors leads to the increased photostability. The residues that we selected are less bulky than the original one (Phe/Leu versus Tyr). The full mechanistic picture of bleaching and photooxidation in FPs is likely to be more complex than the five-state model from Figure 6. For example, we anticipate that other residues may also play a role and that additional ET pathways may be operational (or may become operational upon further mutations). Furthermore, to fully understand oxidative redding in FPs, details of red chromophore formation need to be elucidated. A particularly interesting question concerns catalytic role of various residues in the second step of Scheme 1. Thus, although open questions remain, our results represent the first step toward developing a molecular-level picture of photoinduced ET in FPs and provide motivation for future investigations of this fascinating phenomenon.

4. CONCLUSIONS

By combination of theory and experiment, we identified a dominant pathway for photoinduced ET in FPs by a hopping mechanism via Tyr145. Photooxidation can be efficiently suppressed by disrupting hydrogen bonding between the chromophore and Tyr145 and by π-stacking with Tyr203 (Tyr203 can also serve as an electron acceptor leading to permanent bleaching). The quenching can be controlled by the halide binding. The quenching is explained by (i) changes in energetics of ET between the chromophore and Tyr145 and (ii) the competitive ET channel to Tyr203, which serves as a trap site. The halide binding affects structures, energetics, and electronic couplings. Our mechanism does not exclude possible involvement of other channels; additional pathways for ET and the role of other residues on ET rates will be investigated in the

DOI: 10.1021/jacs.6b00092
J. Am. Chem. Soc. 2016, 138, 4807−4817

future studies. To advance further our understanding of oxidative redding photoconversion, structural information about the red form is needed. A better understanding of the photooxidation mechanism is important for engineering FPs with desired properties optimal for a particular application. Our findings suggest design principles for controlling photoconversions and bleaching via π-stacking and targeted mutations around Tyr145 residue aiming to speed up or slow down ET. We conclude by saying that FPs provide an exciting model for studying mechanism of ET in complex systems such as proteins.

■ ASSOCIATED CONTENT

Supporting Information

The Supporting Information is available free of charge on the ACS Publications website at DOI: 10.1021/jacs.6b00092.

Details of the experimental and computational protocols as well as additional data. (PDF)

Force-field parameters. (PDF)

■ AUTHOR INFORMATION

Corresponding Authors

*kluk@ibch.ru

*krylov@usc.edu

Author Contributions

#A.A. and A.M.B. contributed equally to this work.

Notes

The authors declare no competing financial interest.

■ ACKNOWLEDGMENTS

This work was supported by the U.S. National Science Foundation (CHE-1264018, A.I.K.) and the Russian Science Foundation (14-25-00129, K.A.L.). A.V.M. acknowledges support from the Russian Foundation for Basic Research (16-34-00669-mol-a). The work was partially carried out using the equipment provided by the IBCH Core Facility (CKP IBCH). We thank Dr. Ricardo Matute for performing additional calculations for validating our approach and Professor Arieh Warshel for his advice on the methodology and his comments on the manuscript.

■ REFERENCES

(1) Tsien, R. Y. *Annu. Rev. Biochem.* **1998**, *67*, 509−544.

(2) Chudakov, D. M.; Matz, M. V.; Lukyanov, S.; Lukyanov, K. A. *Physiol. Rev.* **2010**, *90*, 1103−1163.

(3) Shaner, N. C.; Steinbach, P. A.; Tsien, R. Y. *Nat. Methods* **2005**, *2*, 905.

(4) Ha, T.; Tinnefeld, P. *Annu. Rev. Phys. Chem.* **2012**, *63*, 595−617.

(5) Hinterdorfer, P., van Oijen, A., Eds. *Handbook of Single-Molecule Biophysics*; Springer: Dordrecht, 2009.

(6) Lakowicz, J. *Principles of Fluorescence Spectroscopy*, 3rd ed.; Springer: New York, 2009.

(7) Griesbeck, O.; Baird, G. S.; Campbell, R. E.; Zacharias, D. A.; Tsien, R. Y. *J. Biol. Chem.* **2001**, *276*, 29188−29194.

(8) Peterman, E. J. G.; Brasselet, S.; Moerner, W. E. *J. Phys. Chem. A* **1999**, *103*, 10553−10560.

(9) Bogdanov, A. M.; Bogdanova, E. A.; Chudakov, D. M.; Gorodnicheva, T. V.; Lukyanov, S.; Lukyanov, K. A. *Nat. Methods* **2009**, *6*, 859−860.

(10) Bogdanov, A. M.; Kudryavtseva, E. I.; Lukyanov, K. A. *PLoS One* **2012**, *7*, e53004.

(11) Jiménez-Banzo, A.; Ragás, X.; Abbruzzetti, S.; Viappiani, C.; Campanini, B.; Flors, C.; Nonell, S. *Photochem. Photobiol. Sci.* **2010**, *9*, 1336−1341.

(12) Jimenez-Banzo, A.; Nonell, S.; Hofkens, J.; Flors, C. *Biophys. J.* **2008**, *94*, 168.

(13) Bulina, M. E.; Chudakov, D. M.; Britanova, O. V.; Yanushevich, Y. G.; Staroverov, D. B.; Chepurnykh, T. V.; Merzlyak, E. M.; Shkrob, M. A.; Lukyanov, S.; Lukyanov, K. A. *Nat. Biotechnol.* **2006**, *24*, 95−99.

(14) Bulina, M. E.; Lukyanov, K. A.; Britanova, O. V.; Onichtchouk, D.; Lukyanov, S.; Chudakov, D. M. *Nat. Protoc.* **2006**, *1*, 947−953.

(15) Berezin, M. Y.; Achilefu, S. *Chem. Rev.* **2010**, *110*, 2641−2684.

(16) Hofmann, M.; Eggeling, C.; Jakobs, S.; Hell, S. W. *Proc. Natl. Acad. Sci. U. S. A.* **2005**, *102*, 17565−17569.

(17) Burnette, D. T.; Sengupta, P.; Dai, Y.; Lippincott-Schwartz, J.; Kachar, B. *Proc. Natl. Acad. Sci. U. S. A.* **2011**, *108*, 21081−21086.

(18) Nienhaus, K.; Ulrich Nienhaus, G. U. *Chem. Soc. Rev.* **2014**, *43*, 1088−1106.

(19) Lukyanov, K. A.; Serebrovskaya, E. O.; Lukyanov, S.; Chudakov, D. M. *Photochem. Photobiol. Sci.* **2010**, *9*, 1301−1306.

(20) Shcherbakova, D. M.; Verkhusha, V. V. *Curr. Opin. Chem. Biol.* **2014**, *20*, 60−68.

(21) Bogdanov, A. M.; Mishin, A. S.; Yampolsky, I. V.; Belousov, V. V.; Chudakov, D. M.; Subach, F. V.; Verkhusha, V. V.; Lukyanov, S.; Lukyanov, K. A. *Nat. Chem. Biol.* **2009**, *5*, 459−461.

(22) Lukyanov, K. A.; Belousov, V. V. *Biochim. Biophys. Acta, Gen. Subj.* **2014**, *1840*, 745−756.

(23) van Thor, J. J.; Gensch, T.; Hellingwerf, K. J.; Johnson, L. N. *Nat. Struct. Biol.* **2002**, *9*, 37−41.

(24) Grigorenko, B. L.; Nemukhin, A. V.; Morozov, D. I.; Polyakov, I.; Bravaya, K. B.; Krylov, A. I. *J. Chem. Theory Comput.* **2012**, *8*, 1912−1920.

(25) Vegh, R. B.; Bravaya, K. B.; Bloch, D. A.; Bommarius, A. S.; Tolbert, L. M.; Verkhovsky, M.; Krylov, A. I.; Solntsev, K. M. *J. Phys. Chem. B* **2014**, *118*, 4527−4534.

(26) Vegh, R. B.; Solntsev, K. M.; Kuimova, M. K.; Cho, S.; Liang, Y.; Loo, B. L. W.; Tolbert, L. M.; Bommarius, A. S. *Chem. Commun.* **2011**, *47*, 4887−4889.

(27) Grigorenko, B. L.; Nemukhin, A. V.; Polyakov, I.; Khrenova, M. G.; Krylov, A. I. *J. Phys. Chem. B* **2015**, *119*, 5444−5452.

(28) Roy, A.; Field, M. J.; Adam, V.; Bourgeois, D. *J. Am. Chem. Soc.* **2011**, *133*, 18586−18589.

(29) Duan, C.; Adam, V.; Byrdin, M.; Ridard, J.; Kieffer-Jaquinod, S.; Morlot, C.; Arcizet, D.; Demachy, I.; Bourgeois, D. *J. Am. Chem. Soc.* **2013**, *135*, 15841−15850.

(30) Subach, O. M.; Patterson, G. H.; Ting, L.-M.; Wang, Y.; Condeelis, J. S.; Verkhusha, V. V. *Nat. Methods* **2011**, *8*, 771−777.

(31) Pletnev, S.; Shcherbakova, D. M.; Subach, O. M.; Pletneva, N. V.; Malashkevich, V. N.; Almo, S. C.; Dauter, Z.; Verkhusha, V. V. *PLoS One* **2014**, *9*, e99136.

(32) Epifanovsky, E.; Polyakov, I.; Grigorenko, B. L.; Nemukhin, A. V.; Krylov, A. I. *J. Chem. Phys.* **2010**, *132*, 115104.

(33) Wachter, R. M.; Yarbrough, D.; Kallio, K.; Remington, S. J. *J. Mol. Biol.* **2000**, *301*, 157−171.

(34) Nagai, T.; Ibata, K.; Park, E. S.; Kubota, M.; Mikoshiba, K.; Miyawaki, A. *Nat. Biotechnol.* **2002**, *20*, 87−90.

(35) Shcherbo, D.; Souslova, E. A.; Goedhart, J.; Chepurnykh, T. V.; Gaintzeva, A.; Shemiakina, I. I.; Gadella, T. W. J.; Lukyanov, S.; Chudakov, D. M. *BMC Biotechnol.* **2009**, *9*, 24.

(36) Ormö, M.; Cubitt, A. B.; Kallio, K.; Gross, L. A.; Tsien, R. Y.; Remington, S. J. *Science* **1996**, *273*, 1392.

(37) Morris, G. M.; Huey, R.; Lindstrom, W.; Sanner, M. F.; Belew, R. K.; Goodsell, D. S.; Olson, A. J. *J. Comput. Chem.* **2009**, *30*, 2785−2791.

(38) Balabin, I. A.; Hu, X.; Beratan, D. N. *J. Comput. Chem.* **2012**, *33*, 906−910.

(39) Marcus, R. A. *J. Chem. Phys.* **1956**, *24*, 966.

(40) Marcus, R. A. *Annu. Rev. Phys. Chem.* **1964**, *15*, 155.

(41) Olsson, M. H. M.; Hong, G.; Warshel, A. *J. Am. Chem. Soc.* **2003**, *125*, 5025−5039.

DOI: 10.1021/jacs.6b00092
J. Am. Chem. Soc. 2016, 138, 4807−4817

(42) Bravaya, K.; Khrenova, M. G.; Grigorenko, B. L.; Nemukhin, A. V.; Krylov, A. I. *J. Phys. Chem. B* **2011**, *115*, 8296−8303.
(43) Solntsev, K. M.; Ghosh, D.; Amador, A.; Josowicz, M.; Krylov, A. I. *J. Phys. Chem. Lett.* **2011**, *2*, 2593−2597.
(44) Chai, J.-D.; Head-Gordon, M. *J. Chem. Phys.* **2008**, *128*, 084106.
(45) Chai, J.-D.; Head-Gordon, M. *Phys. Chem. Chem. Phys.* **2008**, *10*, 6615−6620.
(46) Phillips, J. C.; Braun, R.; Wang, W.; Gumbart, J.; Tajkhorshid, E.; Villa, E.; Chipot, C.; Skeel, R. D.; Kale, L.; Schulten, K. *J. Comput. Chem.* **2005**, *26*, 1781−1802.
(47) Shao, Y.; Gan, Z.; Epifanovsky, E.; Gilbert, A. T. B.; Wormit, M.; Kussmann, J.; Lange, A. W.; Behn, A.; Deng, J.; Feng, X.; Ghosh, D.; Goldey, M.; Horn, P. R.; Jacobson, L. D.; Kaliman, I.; Khaliullin, R. Z.; Kus, T.; Landau, A.; Liu, J.; Proynov, E. I.; Rhee, Y. M.; Richard, R. M.; Rohrdanz, M. A.; Steele, R. P.; Sundstrom, E. J.; Woodcock, H. L., III; Zimmerman, P. M.; Zuev, D.; Albrecht, B.; Alguire, E.; Austin, B.; Beran, G. J. O.; Bernard, Y. A.; Berquist, E.; Brandhorst, K.; Bravaya, K. B.; Brown, S. T.; Casanova, D.; Chang, C.-M.; Chen, Y.; Chien, S. H.; Closser, K. D.; Crittenden, D. L.; Diedenhofen, M.; DiStasio, R. J., Jr.; Do, H.; Dutoi, A. D.; Edgar, R. G.; Fatehi, S.; Fusti-Molnar, L.; Ghysels, A.; Golubeva-Zadorozhnaya, A.; Gomes, J.; Hanson-Heine, M. W. D.; Harbach, P. H. P.; Hauser, A. W.; Hohenstein, E. G.; Holden, Z. C.; Jagau, T.-C.; Ji, H.; Kaduk, B.; Khistyaev, K.; Kim, J.; Kim, J.; King, R. A.; Klunzinger, P.; Kosenkov, D.; Kowalczyk, T.; Krauter, C. M.; Lao, K. U.; Laurent, A.; Lawler, K. V.; Levchenko, S. V.; Lin, C. Y.; Liu, F.; Livshits, E.; Lochan, R. C.; Luenser, A.; Manohar, P.; Manzer, S. F.; Mao, S.-P.; Mardirossian, N.; Marenich, A. V.; Maurer, S. A.; Mayhall, N. J.; Neuscamman, E.; Oana, C. M.; Olivares-Amaya, R.; O'Neill, D. P.; Parkhill, J. A.; Perrine, T. M.; Peverati, R.; Prociuk, A.; Rehn, D. R.; Rosta, E.; Russ, N. J.; Sharada, S. M.; Sharma, S.; Small, D. W.; Sodt, A.; Stein, T.; Stuck, D.; Su, Y.-C.; Thom, A. J. W.; Tsuchimochi, T.; Vanovschi, V.; Vogt, L.; Vydrov, O.; Wang, T.; Watson, M. A.; Wenzel, J.; White, A.; Williams, C. F.; Yang, J.; Yeganeh, S.; Yost, S. R.; You, Z.-Q.; Zhang, I. Y.; Zhang, X.; Zhao, Y.; Brooks, B. R.; Chan, G. K. L.; Chipman, D. M.; Cramer, C. J.; Goddard, W. A., III; Gordon, M. S.; Hehre, W. J.; Klamt, A.; Schaefer, H. F., III; Schmidt, M. W.; Sherrill, C. D.; Truhlar, D. G.; Warshel, A.; Xu, X.; Aspuru-Guzik, A.; Baer, R.; Bell, A. T.; Besley, N. A.; Chai, J.-D.; Dreuw, A.; Dunietz, B. D.; Furlani, T. R.; Gwaltney, S. R.; Hsu, C.-P.; Jung, Y.; Kong, J.; Lambrecht, D. S.; Liang, W.; Ochsenfeld, C.; Rassolov, V. A.; Slipchenko, L. V.; Subotnik, J. E.; Van Voorhis, T.; Herbert, J. M.; Krylov, A. I.; Gill, P. M. W.; Head-Gordon, M. *Mol. Phys.* **2015**, *113*, 184−215.
(48) Van Voorhis, T.; Kowalczyk, T.; Kaduk, B.; Wang, L.-P.; Cheng, C.-L.; Wu, Q. *Annu. Rev. Phys. Chem.* **2010**, *61*, 149−170.
(49) Foloppe, N.; MacKerell, A. D., Jr. *J. Comput. Chem.* **2000**, *21*, 86−104.
(50) Reuter, N.; Lin, H.; Thiel, W. *J. Phys. Chem. B* **2002**, *106*, 6310−6321.
(51) Wachter, R. M.; Remington, S. J. *Curr. Biol.* **1999**, *9*, R628−R629.
(52) Gray, H. B.; Winkler, J. R. *Q. Rev. Biophys.* **1999**, *36*, 341−372.
(53) Stuchebrukhov, A. A. *Theor. Chem. Acc.* **2003**, *110*, 291−306.
(54) Gray, H. B.; Winkler, J. R. *Proc. Natl. Acad. Sci. U. S. A.* **2005**, *102*, 3534−3539.
(55) Koslowski, T.; Burggraf, F.; Krapf, S.; Steinbrecher, T.; Wittekindt, C. *Biochim. Biophys. Acta, Bioenerg.* **2012**, *1817*, 1955−1957.
(56) Beratan, D. N.; Liu, C.; Migliore, A.; Polizzi, N. F.; Skourtis, S. S.; Zhang, P.; Zhang, Y. *Acc. Chem. Res.* **2015**, *48*, 474−481.
(57) Wittekindt, C.; Schwarz, M.; Friedrich, T.; Koslowski, T. *J. Am. Chem. Soc.* **2009**, *131*, 8134−8140.
(58) Isse, A. A.; Gennaro, A. *J. Phys. Chem. B* **2010**, *114*, 7894.
(59) Hosoi, H.; Hazama, S.; Takeda, Y. *Chem. Phys. Lett.* **2015**, *618*, 186−191.
(60) Mena, M. A.; Treynor, T. P.; Mayo, S. L.; Daugherty, P. S. *Nat. Biotechnol.* **2006**, *24*, 1569−1571.
(61) Ai, H. W.; Shaner, N. C.; Cheng, Z.; Tsien, R. Y.; Campbell, R. E. *Biochemistry* **2007**, *46*, 5904−5910.
(62) Shaner, N. C.; Lin, M. Z.; McKeown, M. R.; Steinbach, P. A.; Hazelwood, K. L.; Davidson, M. W.; Tsien, R. Y. *Nat. Methods* **2008**, *5*, 545−551.
(63) Zhong, S.; Navaratnam, D.; Santos-Sacchi, J. *PLoS One* **2014**, *9*, e99095.
(64) McAnaney, T. B.; Zeng, W.; Doe, C. F. E.; Bhanji, N.; Wakelin, S.; Pearson, D. S.; Abbyad, P.; Shi, X.; Boxer, S. G.; Bagshaw, C. R. *Biochemistry* **2005**, *44*, 5510−5524.
(65) Dean, K. M.; Lubbeck, J. L.; Binder, J. K.; Schwall, L. R.; Jimenez, R.; Palmer, A. E. *Biophys. J.* **2011**, *101*, 961−969.
(66) Drobizhev, M.; Hughes, T. E.; Stepanenko, Y.; Wnuk, P.; O'Donnell, K.; Scott, J. N.; Callis, P. R.; Mikhaylov, A.; Dokken, L.; Rebane, A. *Sci. Rep.* **2012**, *2*, 688.
(67) Pletnev, S.; Gurskaya, N. G.; Pletneva, N. V.; Lukyanov, K. A.; Chudakov, D. M.; Martynov, V. I.; Popov, V. O.; Kovalchuk, M. V.; Wlodawer, A.; Dauter, Z.; Pletnev, V. *J. Biol. Chem.* **2009**, *284*, 32028−32039.
(68) Carpentier, P.; Violot, S.; Blanchoin, L.; Bourgeois, D. *FEBS Lett.* **2009**, *583*, 2839−2842.
(69) de Rosny, R.; Carpentier, P. *J. Am. Chem. Soc.* **2012**, *134*, 18015−18021.

DOI: 10.1021/jacs.6b00092
J. Am. Chem. Soc. 2016, 138, 4807−4817